The Estuarine Circulation

W. Rockwell Geyer[1] and Parker MacCready[2]

[1]Woods Hole Oceanographic Institution, Woods Hole, Massachusetts 02543; email rgeyer@whoi.edu

[2]School of Oceanography, University of Washington, Seattle, Washington 98195-5351; email: pmacc@uw.edu

Annu. Rev. Fluid Mech. 2014. 46:175–97

First published online as a Review in Advance on August 26, 2013

The *Annual Review of Fluid Mechanics* is online at fluid.annualreviews.org

This article's doi: 10.1146/annurev-fluid-010313-141302

Keywords

residual circulation, exchange flow, tidal straining, isohaline coordinates, parameter space

Abstract

Recent research in estuaries challenges the long-standing paradigm of the gravitationally driven estuarine circulation. In estuaries with relatively strong tidal forcing and modest buoyancy forcing, the tidal variation in stratification leads to a tidal straining circulation driven by tidal variation in vertical mixing, with a magnitude that may significantly exceed the gravitational circulation. For weakly stratified estuaries, vertical and lateral advection are also important contributors to the tidally driven residual circulation. The apparent contradiction with the conventional paradigm is resolved when the estuarine parameter space is mapped with respect to a mixing parameter M that is based on the ratio of the tidal timescale to the vertical mixing timescale. Estuaries with high M values exhibit strong tidal nonlinearity, and those with small M values show conventional estuarine dynamics. Estuaries with intermediate mixing rates show marked transitions between these regimes at timescales of the spring-neap cycle.

1. INTRODUCTION: CLASSICAL TIDALLY AVERAGED BALANCES IN ESTUARINE CIRCULATION AND SALINITY STRUCTURE, AND WHY THEY ARE BEING CHALLENGED

Exchange flow: another term for the estuarine circulation, but emphasizes that the subtidal along-channel flow is commonly structured in space, with persistent inflow of deeper water and persistent outflow above, and that this transport may be primarily responsible for exchanging water between the estuary and the ocean

Estuarine circulation: the most general term for the tidally averaged along-channel velocity through an estuarine cross section

Tidally averaged or subtidal: denotes that a time series of the property referred to (e.g., subtidal salinity) has had a low-pass filter applied to it, averaging out variation at tidal and higher frequencies; the term residual is often applied synonymously

An estuary, broadly defined, is any embayment of the coast in which buoyancy forcing alters the fluid density from that of the adjoining ocean. These systems can be fjords, drowned river valleys, bar-built estuaries, and rias, among others (Valle-Levinson 2010). The buoyancy source is usually a river or rivers but can also be heating, evaporation, or the freezing and melting of ice. This review focuses on river-forced systems, in which the buoyancy forcing is positive. The buoyancy forcing naturally gives rise to a horizontal density gradient and hence a horizontal pressure gradient. The other main actor in the drama is turbulent mixing, driven primarily by tidal currents and wind. Mixing distributes the buoyancy contrast deeper in the water column inside the estuary. This buoyant volume continually rises and flows out of the estuary mouth in part because the pressure gradient tries to flatten both isopycnals and the free surface. On the coast, the result is a river plume.

At the mouth of the estuary, dense shelf water is drawn in to replace the escaping mixture, meaning that below the outflowing surface layer, the deeper water is flowing into the estuary. This bidirectional flow is called the exchange flow, referred to by many authors as the estuarine circulation. In this article, we treat the two terms as synonyms. Although the exchange flow is typically an order of magnitude weaker than the tidal flow, it is of disproportionate importance with respect to the distribution of waterborne material. The exchange flow greatly augments the longitudinal dispersion of passive tracers relative to an embayment without significant buoyancy input, but it effectively traps particles that sink, such as sediment or particulate organic matter. The consequences of rapid flushing are the rapid dispersion of dissolved contaminants (Smith 1976) and high biological productivity (Malone et al. 1988). The consequences of trapping are high sediment accumulation rates (Traykovski et al. 2004), extensive nutrient recycling (Hopkinson et al. 1999), and frequent hypoxia and acidification of the deep water (Paerl et al. 1998, Feely et al. 2010). Quantified as a volume transport, the inflowing branch of the exchange flow is often many times greater than that of the river flow, emphasizing its importance.

There is thus clear biogeochemical motivation to study the physics of the exchange flow, and logically this has focused on the tidally averaged momentum balance of the along-channel flow. For a known bathymetry, river flow, and distribution of tidal currents, we would like to predict the exchange flow and associated density field. An early consensus on the important terms in the momentum balance emerged in the 1950s, wherein the baroclinic pressure gradient balanced the vertical divergence of stress. Tides appeared mainly as a driver for turbulence, seemingly amenable to parameterization, and successful analytical solutions emerged, as reviewed in MacCready & Geyer (2010).

There is, however, good reason to be skeptical of these solutions because the exchange flow they try to predict is a small residual of the tidal current. Typical scales are 0.1 m s^{-1} for the tidally averaged (also called residual or subtidal) current, compared with 1 m s^{-1} for the tide. The first hint of tidal trouble for classical theories arises in the along-channel salt balance, in which the tidal-timescale correlation of salinity with tidal currents is parameterized using an ad hoc along-channel diffusivity. In tidally energetic systems, over half the subtidal along-channel salt flux may be ascribed to this term (Hughes & Rattray 1980).

This is not the only problem that arises when taking the tidal average. Although it is perhaps more tractable than the salt balance, the tidally averaged momentum balance is subject to a suite of influences of tidal processes that have received considerable attention in recent years. This is not unexpected: Tidal currents have along-channel momentum of both signs with scale an order of magnitude greater than the residual. Any process, especially cross-channel and vertical advection

or mixing of momentum, that is not in perfect temporal quadrature with the tides will appear in the Eulerian tidally averaged along-channel momentum balance, potentially at leading order. It has been found that these terms are especially important in systems in which mixing is strong enough to destratify the water column during part of the tidal cycle.

In the following, we summarize recent results, primarily from idealized numerical simulations, that show when and where a fundamental rethinking of the momentum dynamics of the estuarine circulation is required. This motivates a consideration of the dimensionless parameters that describe estuarine dynamical regimes. We also place these new momentum results in context with the system-wide salt balance and the mechanisms that create the salinity gradient. This involves the spring-neap and event-driven system response. New results from calculating residual transports using a moving isohaline coordinate system are also reviewed. Finally, we consider whether our new physical understanding leads to better parameters for the prediction of the magnitude of the exchange flow across a wide diversity of estuarine systems.

2. CLASSICAL ANALYSIS OF ESTUARINE CIRCULATION

Estuaries are complex systems, with nonlinear coupling and feedback between the circulation and density structure. A prominent line of theoretical inquiry has sought to predict system-wide properties, such as the length of the salt intrusion. However, to make progress in untangling the momentum balance itself, researchers have been prompted to simplify the problem, focusing instead on local dynamics at a single cross section of a long channel. The channel bathymetry may have cross-channel variation, but along-channel variation is assumed negligible. Moreover, the along-channel salinity gradient is assumed to be known and constant on the cross section. Even within this simple idealization, complex dynamical interactions arise that provide the foundations of our understanding of estuarine momentum dynamics.

2.1. The Residual Circulation with Constant Eddy Viscosity, One Dimension

We begin with a brief rederivation of the classical balances. The mathematical manipulations and decomposition concepts presented here are identical to those used when adding new processes, and so are a useful starting point. The Reynolds-averaged equations for salinity and along-channel momentum, in hydrostatic form and subject to the Boussinesq approximation, may be written as

$$\frac{\partial s}{\partial t} + \mathbf{u} \cdot \nabla s = \frac{\partial}{\partial z}\left(K \frac{\partial s}{\partial z}\right), \tag{1}$$

$$\frac{\partial u}{\partial t} + \mathbf{u} \cdot \nabla u - fv = -g\frac{\partial \eta}{\partial x} - \frac{\partial}{\partial x}\int_z^\eta \frac{g\rho}{\rho_0} d\hat{z} + \frac{\partial}{\partial z}\left(A\frac{\partial u}{\partial z}\right), \tag{2}$$

where s is salinity, the velocity is $\mathbf{u} = (u, v, w)$, and $\mathbf{x} = (x, y, z)$, where x is along channel (flood positive), y is cross channel, and z is positive up with zero at the rest-state free surface (**Figure 1*a***). The Coriolis frequency is f, g is gravity, and the free surface is at $\eta(x, y, t)$. The first two terms on the right-hand side of Equation 2 are the pressure gradient force per unit mass, assumed hydrostatic, with density $\rho = \rho_0(1+\beta s)$, where ρ_0 is a constant background density (freshwater) and $\beta \cong 7.7 \times 10^{-4}$. The eddy viscosity is $A(\mathbf{x}, t)$ and eddy diffusivity $K(\mathbf{x}, t)$. The tidal variability of these quantities provides the basis for the discussion in the next section, but the classical analysis assumes that constant values of the mixing coefficients can be applied to the tidally averaged dynamics.

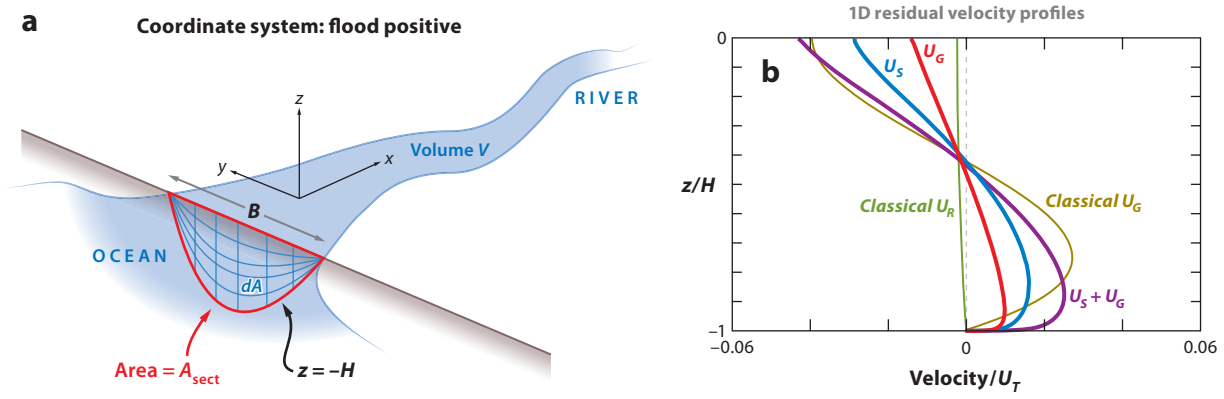

Figure 1

(*a*) Definition sketch of the estuarine volume and cross section. (*b*) Plot of the normalized residual velocity profiles for two classes of 1D solutions versus normalized depth. The thin lines are from the classical solution (Equation 8). The three thicker lines are from a numerical simulation within the strain-induced periodic stratification regime. In this regime, the strain-induced circulation is about twice as large as the gravitational circulation, although neither is very large. Panel *b* adapted with permission from Burchard & Hetland (2010, figure 3, central panel), copyright American Meteorological Society.

Proceeding toward the classical balances, we neglect momentum advection (for now) and Coriolis forces. We assume that free surface changes are negligible, except as their gradients provide an along-channel body force. To simplify the notation, we define the buoyancy $b \equiv -g(\rho - \rho_0)/\rho_0$ and denote partial derivatives with subscripts x, y, z, and t. We assume b_x to be constant and known; hence this is a local solution without reference to how b_x is set or maintained. Under these assumptions, Equations 1 and 2 may be written as

$$s_t + us_x = (Ks_z)_z \quad \text{or} \quad b_t + ub_x = (Kb_z)_z, \tag{3}$$

$$u_t = -g\eta_x - zb_x + (Au_z)_z. \tag{4}$$

Note that $b_x = -g\beta s_x$, so salt and buoyancy gradients are essentially synonymous. Taking the tidal average, denoted by angle brackets, of Equation 4, we find

$$0 = -g\langle\eta_x\rangle - zb_x + \langle Au_z\rangle_z. \tag{5}$$

The earliest solutions (e.g., Hansen & Rattray 1965) assumed that this balance was the same across the width of the channel or that it applied to width-averaged quantities, so it is essentially a one-dimensional (1D) problem, varying only in z. The other classical assumption is that we may linearize the stress divergence term by defining an effective eddy viscosity $A_{\text{eff}}\langle u_z\rangle \equiv \langle Au_z\rangle$ and assuming that A_{eff} is constant. In practice, A_{eff} became a tuning parameter for fitting the theory to observations, and in many cases it worked surprisingly well (Hansen & Rattray 1965, MacCready 2004). Ralston et al. (2008) developed a parameterization for the effective viscosity in terms of the tidal currents and b_x that showed good skill in the Hudson River estuary. But this simplification has proven to be one of the key points of contention with the classical balance (see Section 3).

Gravitational circulation: similar to exchange flow, but assumes that the primary driving force creating the circulation is the baroclinic pressure gradient

With this caution in mind, we finish the classical derivation. Following the procedure of Burchard & Hetland (2010) and Cheng et al. (2010), we decompose the subtidal velocity into a part associated with the river flow and a part associated with the gravitational circulation (i.e., driven by b_x): $\langle u\rangle = u_R + u_G$. The subtidal surface height gradient is likewise decomposed as $g\langle\eta_x\rangle = G_R + G_G$. Equation 5 may then be written as a pair of second-order ordinary differential

equations:

$$0 = -G_R + \partial(A_{\text{eff}}\partial u_R/\partial z)/\partial z,$$
$$0 = -G_G - zb_x + \partial(A_{\text{eff}}\partial u_G/\partial z)/\partial z. \quad (6)$$

These are solved by first integrating vertically from z to the free surface and applying a no-stress boundary condition. Had we wished to include wind stress, there would have been a third term in the decomposition, and the stress would have been applied only to it (Ralston et al. 2008, Burchard & Hetland 2010). Dividing the results by A_{eff}, we find equations for the residual velocity components,

$$\partial u_R/\partial z = G_R z/A_{\text{eff}},$$
$$\partial u_G/\partial z = G_G z/A_{\text{eff}} + z^2 b_x/(2A_{\text{eff}}). \quad (7)$$

Next we integrate from the bottom at $z = -H$ up to position z and assume that a no-slip bottom boundary condition applies to both terms of the decomposed velocity. Finally, we choose values of G_R and G_G such that the vertical integral of u_R carries the river volume transport, and u_G has zero vertical integral. For A_{eff} constant in z, these values result in the classical parabolic and cubic profiles shown by the thin lines in **Figure 1*b***and given by MacCready & Geyer (2010):

$$\langle u \rangle = u_R + u_G = -U_R(1.5 - 1.5\zeta^2) - U_G(1 - 9\zeta^2 - 8\zeta^3), \quad (8)$$

where $\zeta \equiv z/H$, U_R is the river volume flux divided by A_{sect}, and the strength of the gravitational circulation is $U_G = b_x H^3/(48A_{\text{eff}})$. The utility of the decomposition is that it cleanly separates the velocity into profiles that are controlled by distinct physical processes. The profile of u_R depends only on the river flow, and the profile of u_G depends only on b_x, although both are still affected by A_{eff} and H. This utility will prove essential as the decomposition is extended to include other physical processes. We must also be aware, however, that the decomposition is not unique—the solutions are very much affected by the choices made for boundary conditions and integral constraints.

2.2. Scaling of the Eddy Viscosity

The variability of the eddy viscosity A is the crux of the problem of quantifying the estuarine circulation. In particular, the sensitivity of A to stratification makes its value vary by as much as three orders of magnitude, from a value of approximately 500×10^{-4} m^2 s^{-1} in unstratified, maximum tidal flow conditions (Dyer & Soulsby 1988) to less than 1×10^{-4} m^2 s^{-1} within the stratified pycnocline (Peters & Bokhorst 2001). Following conventional unstratified boundary layer scaling,

$$A = \kappa u_* z(1 - z/H), \quad (9)$$

where $\kappa = 0.4$ is von Kármán's constant, and z here is the height above the bottom (Nezu & Rodi 1986). The boundary stress may be estimated as $u_*^2 = C_D U_T^2$, where $C_D \cong (1\text{–}2.5) \times 10^{-3}$ and U_T is the amplitude of the depth-averaged tidal velocity. The mid-depth maximum value is $A_{\max} \cong 0.005 U_T H$, yielding the very high values of A mentioned above.

Stratification greatly reduces A, mainly by limiting the vertical length scale of turbulent eddies. Numerous closure approaches have been used to represent the influence of stratification, many of which include some quantity related to the gradient Richardson number $Ri = N^2/u_z^2$, where $N^2 = -(g/\rho_0)\rho_z$, as reviewed in Umlauf & Burchard (2005). These formulations have proven to be effective in prognostic calculations of estuarine dynamics (e.g., Warner et al. 2005, Li & Zhong 2009). However, none of these approaches is particularly effective for approximate scaling of the magnitude of A in estuaries because they require knowledge of the local stratification and shear, often the quantities that we are interested in estimating. Nonetheless, using a mixing length

argument to estimate the eddy viscosity, we find that $A \sim u_* L_{\text{turb}}$, where L_{turb} is a turbulent length scale. L_{turb} scales like $\kappa z \sim \kappa H/4$ in unstratified channel flow but may be orders of magnitude smaller in stratified flows. Roughly it follows Ozmidov scaling, $L_{\text{turb}} \sim u_*/N$ (Scully et al. 2011), with typical values $L_{\text{turb}} = 5$–20 cm for moderately stratified estuaries.

2.3. The Salt Balance and Buoyancy Gradient

In the discussion of the dynamics above, the along-estuary salinity gradient is prescribed. In actual estuaries, the salinity gradient is part of the solution of the coupled salt and momentum equations. The classic formulation for the subtidal salt balance by Hansen & Rattray (1965) divided the salt transport into a seaward-directed component due to the river outflow and two landward components, one due to the estuarine circulation and the other due to tidal dispersion. The salt balance, integrated over the estuarine volume starting at any cross section, may be written in the notation of Lerczak et al. (2006) as

$$\frac{d}{dt}\left\langle \int sdV \right\rangle = \left\langle \int usdA \right\rangle = u_0 s_0 A_0 + \int u_1 s_1 dA_0 + \left\langle \int u_2 s_2 dA \right\rangle, \tag{10}$$

where the subscript 0 denotes a property that has been tidally averaged and then averaged over a cross section, the subscript 1 denotes a property that has been tidally averaged but varies over the section (e.g., vertical stratification), and the subscript 2 denotes the tidally and sectionally varying remainder. The first term on the right-hand side is the loss of salt due to the river flow ($u_0 \cong -U_R$). The second term on the right-hand side is the salt flux due to the exchange flow ($u_1 = u_G$ for the classical solution). The final term on the right-hand side is the tidal salt flux, typically parameterized using a Fickian diffusion with very large diffusivity, $O(100$–$1{,}000\ \text{m}^2\ \text{s}^{-1})$ (MacCready 2004, 2011).

The salt flux of the second term, $\int u_1 s_1 dA_0$, clearly depends on the strength of u_G, which, as seen above, varies with b_x. Nonzero s_1 requires subtidal stratification, which in turn is forced by straining of the along-channel salinity gradient by the estuarine circulation, $s_{zt} \propto (\partial u_G/\partial z)(\partial s_0/\partial x)$, and hence varies as b_x^2. The salt flux due to their product will vary as b_x^3 (MacCready & Geyer 2010). We then note that the upestuary salt flux balances the river flow U_R, so the along-estuary gradient b_x should vary as $U_R^{1/3}$. Given that power-law relationship, the stratification should vary as $U_R^{2/3}$ (MacCready 1999, Hetland & Geyer 2004, MacCready & Geyer 2010), which is consistent with our expectations that estuaries become more strongly stratified for stronger river outflow. Contrary to intuition, these equations do not produce a dependence of stratification on tidal velocity; this is because b_x varies linearly as U_T, which compensates for the intensified mixing (MacCready 1999). As discussed in Section 4, the time dependence of the estuarine salt balances relaxes the assumptions leading to these relationships and produces a wide range of transient solutions, but these relationships define the equilibrium regime, in which b_x has adjusted to bring salt and momentum into local and global balance.

In summary, the salt content of the estuary and the associated salinity gradient $\partial s/\partial x$ will vary owing to the variations in the river outflow, the exchange flow, and tidally induced salt transport processes. The river outflow has a relatively simple impact on the salt balance—increased river flow pushes the salt intrusion seaward and increases $\partial s/\partial x$. How much it increases $\partial s/\partial x$ is complicated by the amplitude of the response of the exchange flow and tidal salt transports to changes in $\partial s/\partial x$. The classic Hansen & Rattray (1965) or Chatwin (1976) solutions rely on an assumed form of the momentum balance, one that obeys Equation 7 and in which the exchange flow is forced by the baroclinic gradient b_x. It is this assumption that is being challenged.

3. ESTUARINE CIRCULATION WITH TIDALLY VARIABLE MIXING

The preceding section stresses the importance of the vertical shear of the subtidal velocity to the creation of stratification. Since the groundbreaking work on strain-induced periodic stratification (SIPS), it has been recognized that the tidal variation of stratification caused by advection, $s_{zt} = -u_z s_x$, where u_z is the tidally varying shear, may have important dynamic consequences as well (van Aken 1986, Simpson et al. 1990). The increased stratification at the end of the ebb tide should decrease vertical mixing, and conversely, late flood mixing should be enhanced by convective instability in the bottom boundary layer. Based on this hypothesized variation in mixing, Jay & Musiak (1994) suggested that the flood tide momentum would be preferentially mixed downward more effectively than the ebb tide momentum. The effect on the residual flow would be similar to the effect of baroclinicity in classical gravitational circulation: deep water flowing in and surface water moving out. This new effect has been given different names by different investigators; here we follow Burchard et al. (2011), calling it the tidal straining circulation. We begin by considering the scaling of processes with tidal variability.

3.1. The Simpson Number and Competition Between Straining and Mixing on an Ebb Tide

Van Aken (1986) and Simpson et al. (1990) considered the energetics of turbulence in the presence of tidal straining. Based on their analysis, the ratio of potential energy change due to straining to the rate of production of turbulent kinetic energy can be expressed as

$$b_x H^2/(C_D U_T^2) \equiv Si. \tag{11}$$

This is the Simpson number, named in honor of John Simpson (Stacey et al. 2010, Burchard et al. 2011). The Simpson number has also been called the horizontal Richardson number, Ri_x (Monismith et al. 1996, Stacey 1996, Stacey et al. 2001). For small values of Si, the kinetic energy of the turbulence can overcome the stabilizing influence of tidal straining during the ebb tide, leading to vertically well-mixed conditions. For intermediate values of Si, the SIPS regime occurs, with stratification taking place during some portion of the ebb and the water column becoming well mixed during the flood tide. For high values of Si, runaway stratification occurs, as discussed below. Stacey & Ralston (2005) found that $Si \sim 0.2$ represents a transition to permanently stratified conditions during the ebb tide, in which vertical mixing is stabilized by strain-induced stratification. For smaller values of Si, full water-column mixing can occur even during the ebb tide, subject to the constraint that there is enough time within the tide for boundary layer mixing to extend through the water column.

3.2. The Growth of the Bottom Mixed Layer and the Mixing Number

Neglecting for the moment the influence of horizontal density gradients, the rate of growth of the estuarine boundary layer can be parameterized analogously with the growth of an oceanic wind-mixed layer

$$\frac{dh_{\mathrm{bl}}}{dt} = C\frac{u_*^2}{N_\infty h_{\mathrm{bl}}}, \tag{12}$$

where h_{bl} is the boundary layer thickness, and $C \approx 0.6$ is a constant related to the mixing efficiency (Kato & Phillips 1969, Trowbridge 1992). N_∞ is the stratification above the bottom boundary layer. Considering uniform stratification as an initial condition, one can integrate Equation 12, substituting for u_* using the quadratic drag of the tidal flow, to obtain an estimate of the conditions

in which the mixed layer will penetrate through the entire water column within one-half tidal cycle:

$$\frac{C_D U_T^2}{\omega N_\infty H^2} \approx 1, \tag{13}$$

where ω is the tidal frequency. The dependence of mixing on the tidal frequency was highlighted by Burchard & Hetland (2010) and Burchard et al. (2011), with the latter defining an unsteadiness number

$$Un \equiv \frac{\omega H}{u_*}, \tag{14}$$

which conveys the importance of the unsteadiness of boundary layer mixing in the absence of stratification. The expression in Equation 13 conveys the inhibiting influence of stratification, which slows down vertical mixing and increases the adjustment timescale for a given tidal velocity. The parameterization for tidal mixing is revisited in a discussion of the estuarine parameter space in Section 5. Returning now to the issue of tidal straining, the rate of destratification increases during the flood tide and decreases during the ebb tide. Following similar arguments about the balance of buoyancy flux and turbulent kinetic energy production that lead to the definition of *Si*, the rate of mixed layer deepening should be adjusted by the factor $1 \pm \gamma Si$, where γ is a factor that depends on the ratio of the efficiency of straining to the efficiency of vertical mixing, the minus sign applies to stabilizing ebb shear, and the plus sign applies to destabilizing flood shear. Stacey & Ralston (2005) suggested a value of $\gamma \sim 5$, based on a turbulent mixing efficiency $R_f \sim 0.2$, which would suggest that permanent stratification should occur when $Si > 0.2$. This is consistent with the model results of Burchard et al. (2011), which produce runaway stratification for $Si > 0.2$. However, Stacey & Ralston's estimate assumed log-layer scaling for shear, which may not be valid for flows with significant stratification. More analysis of field measurements and models under varying stratification conditions should be performed to firm up the appropriate value of γ under different circumstances.

3.3. Forcing of Residual Circulation by the Tidal Variation of Mixing

Based on the above scaling arguments as well as observations (Simpson et al. 1990, Stacey et al. 2001, Stacey & Ralston 2005), estuaries with low values of *Si* (~0.1–0.3) will exhibit significant tidal variation in stratification, with complete destratification during flood tides and at least partial restratification during ebb tides. This periodically destratified region of estuarine parameter space is thus subject to the strong asymmetry of the magnitude of the eddy viscosity (**Figure 2**). Because of enhanced mixing, the shears are weaker during flood tides than ebb tides, and there is a notable reversal of shear at the end of ebb tides owing to the combination of the vertical phase shift in tidal velocity and baroclinicity during an interval of weak $A(z)$.

The strength of the tidal straining effect has recently been rigorously explored in this part of parameter space by Burchard & Hetland (2010). Using a 1D (z, t) numerical model with a rigid lid and modern turbulence closure scheme, the authors performed a number of experiments varying the tidal velocity and along-channel density gradient. To analyze their experiments, they decomposed the resulting subtidal circulation using methods identical to those described in Section 2.1 but explicitly pulling out the time-varying shear stress. The tidally averaged vertical stress in Equation 5 may be decomposed as

$$\langle A u_z \rangle = \langle A' u_z' \rangle + \langle A \rangle \langle u_z \rangle, \tag{15}$$

where a prime denotes the deviation from a tidally averaged quantity. The subsequent decomposition and solution procedure are the same as in the classical case, except that now we divide each

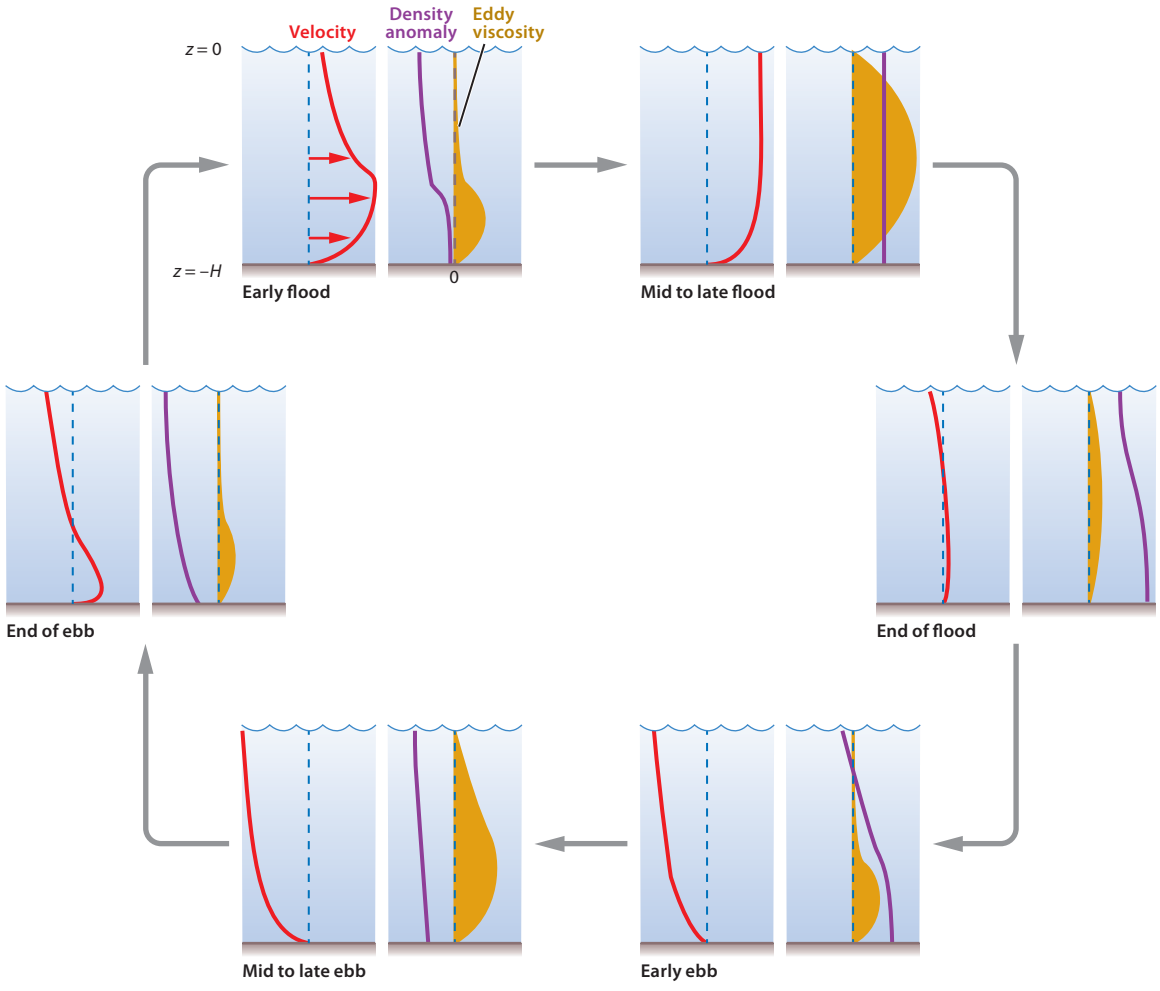

Figure 2

Profiles of velocity, density anomaly, and eddy viscosity as they evolve over a tidal period for the strain-induced periodic stratification regime, where there is complete destratification during the flood tide, leading to strong mixing and almost no vertical shear. In contrast, the ebb tide may develop substantial shear owing to the suppression of turbulence by stratification, which originates from the straining of the horizontal density gradient. The stratification at the end of the flood tide results from lateral straining, whereas the increasing stratification during the ebb tide results from along-estuary straining.

term by $\langle A \rangle$ instead of A_{eff}, and there is a new term, identified in Burchard & Hetland (2010) as a physical forcing term for a residual velocity component u_S associated with tidal straining. The resulting equations for the three velocity components, analogous to Equation 7, are as follows:

$$\begin{aligned} \partial u_R/\partial z &= G_R z/\langle A \rangle, \\ \partial u_G/\partial z &= G_G z/\langle A \rangle + z^2 b_x/(2\langle A \rangle), \\ \partial u_S/\partial z &= G_S z/\langle A \rangle - \langle A' u'_z \rangle/\langle A \rangle. \end{aligned} \tag{16}$$

The solution is no longer analytically tractable, so Burchard & Hetland (2010) derived the profiles from idealized numerical solutions in which the tidal variation of the shear stress is resolved.

What they found (**Figure 1*b***) is the remarkable result that u_S generally has the same vertical shape as u_G; both look like an exchange flow, but the velocity forced by tidal straining is twice as large as that driven by the gravitational circulation! This result represents such a strong challenge to the classical understanding that it merits careful attention.

Burchard & Hetland (2010) demonstrated that the tidal straining circulation scales approximately linearly with *Si*, with the approximate result that $U_E/U_T = 0.2Si$ for *Si* values between 0.12 and 0.28. The classical gravitational circulation also scales linearly with *Si*, and based on the Ralston et al. (2008) parameterization ($A_{\text{eff}} = 0.028C_D U_T H$), this leads to $U_G/U_T = 0.8Si$ for permanently stratified estuaries. Thus we have the paradoxical result that tidal straining circulation dominates gravitational circulation for small *Si*, but for permanently stratified estuaries, the gravitational circulation is roughly four times stronger than the tidal straining circulation for a given value of *Si*. The stronger response of permanently stratified estuaries is a consequence of the marked reduction of A_{eff} with stratification, which occurs only for a small fraction of the tidal cycle in the tidal straining regime. The transition between the tidal straining regime and the permanently stratified regime has proven difficult to analyze because of runaway stratification, discussed below.

The other crucial consideration here is that the physical interpretation of u_S poses some difficulties. Whether $\langle A' u_z' \rangle_z$ should be interpreted as a forcing mechanism in Equation 16 is the subject of ongoing debate in the field. A valid complaint (Stacey et al. 2010) against the use of A_{eff} was that, when allowed to have vertical structure, it turned out to be negative over much of the water column. Similarly, A' is by definition negative over half the tidal cycle. Nevertheless, the results of Burchard & Hetland (2010) conclusively demonstrate that the tidal variation of A has leading-order consequences in the periodically destratified regime. A final comment is that in the extreme limit of strong *M*, and small *Si*, the system is always well mixed, A has little tidal asymmetry, and little exchange flow of any kind is expected, posing difficulties for the global salt balance (Equation 10).

3.4. Time-Dependent Response: Runaway Stratification and the Spring-Neap Cycle

A distinctive characteristic of 1D and 2D models of the estuarine circulation is runaway stratification (Simpson et al. 1990, Monismith et al. 2002, Burchard & Hetland 2010, Cheng et al. 2010, Burchard et al. 2011), which occurs at a high-enough value of *Si* that the straining of the density gradient overtakes mixing, resulting in an unbounded increase in stratification and exchange flow. The phenomenon occurs because of the strong nonlinearity of the stratification equation, particularly when the stabilizing influence of stratification is considered (Monismith et al. 2002). The *Si* value at which this occurs is not particularly high—approximately 0.2 for the numerical experiments of Burchard et al. (2011), which is well within the normal range of values observed in partially mixed estuaries (Stacey & Ralston 2005). If runaway stratification occurs in 1D models, why does it not occur in nature?

The answer is that it does. Many, perhaps most, partially mixed estuaries show significant variations in stratification through the spring-neap cycle. This phenomenon was first described by Haas (1977) and has since been documented in a great variety of regimes, including fjords (Geyer & Cannon 1982, Griffin & LeBlond 1990), partially mixed estuaries (Sharples & Simpson 1993, Uncles & Stephens 1993, Monismith et al. 1996), and even salt-wedge regimes (Jay & Smith 1990). For transitional estuaries such as these, the Simpson number increases above the runaway threshold ($Si \sim 0.2$) during neap tides, indicating that the potential energy input due to straining by the mean gravitational circulation exceeds the buoyancy flux due to tidal mixing. This allows

the stratification to increase, which further isolates boundary layer mixing from the overlying water column, accelerating the transition to stable conditions.

The runaway condition is not as extreme in real estuaries as in 1D and 2D models because the along-channel density gradient is not constant and instead decreases as the salt intrusion extends during neap conditions. As discussed in Section 2, the equilibrium length of the estuary depends inversely on the intensity of mixing (MacCready 1999), so as the mixing decreases during neaps, the estuary adjusts toward that new equilibrium, with a corresponding reduction in $\partial s/\partial x$. Depending on the response timescale of the estuary (MacCready 1999, 2007; Lerczak et al. 2009), the estuarine length may not fully adjust in the timescale of the spring-neap cycle (Hetland & Geyer 2004), but in any case, $\partial s/\partial x$ will adjust downward in response to the reduction of tidal mixing energy.

The mechanics of the spring-neap transitions have not been fully explained—particularly the return to stratified conditions after an estuary becomes well mixed. Numerical simulations in one dimension (vertical) by Nunes Vaz et al. (1989) indicated there was a 2–3-day lag in restratification after neap tides, owing to the time required for stratification to become re-established from well-mixed conditions. Observations by Haas (1977) of subestuaries of Chesapeake Bay indicate there are lags consistent with Nunes Vaz et al. (1989), but observations in the Hudson estuary by Geyer et al. (2000) indicate that restratification is much more rapid than would be expected only in the presence of uniform, along-estuary straining. One reason for the rapid restratification is lateral straining, which occurs at the end of the flood tide in well-mixed estuaries (Nunes & Simpson 1985). This rapid restratification process may explain the short lag observed in the transition back to stratified conditions in relatively narrow estuaries.

Another aspect of the restratification process that is not captured in 1D or 2D (z or y-z) models is frontogenesis. A recent modeling study by Ralston et al. (2012) of the Hudson estuary indicates that the transition from weak to strong stratification is initiated at specific locations within the estuary at which fronts develop during the late ebb tide. The mechanism of frontogenesis is consistent with the theoretical and laboratory study by Simpson & Linden (1989), in which a local maximum in $\partial s/\partial x$ was amplified by the baroclinicity during an interval of weak tidal mixing, leading to intensification of the gradient, development of exchange flow, and increased stratification. Ralston et al.'s (2012) model results indicate that topographic variation—a significant increase in either the depth or width in the out-estuary direction—favors the intensification of the near-bottom salinity gradient at the end of the ebb tide and the initiation of frontogenesis. Their model simulations indicate that after such fronts form during the transition to neap tide conditions, they propagate upstream during subsequent flood tides, leading to restratification of the entire salt intrusion through the course of the neap tide (**Figure 3**). These results suggest that the spring-to-neap transition does not happen uniformly but rather that frontogenesis and frontal propagation may be integral to this transition process.

4. TWO- AND THREE-DIMENSIONAL SOLUTIONS

Although the strict focus on vertically varying processes above is important, the strong dependence of the results on channel depth suggests that a more complete consideration of the effects of varying bathymetry is needed.

4.1. The Influence of Secondary Circulation: The Advectively Driven Circulation

The lateral dimension has important effects on the estuarine circulation, resulting from both the lateral structure of the along-channel flow and the influence of lateral advection on the momentum

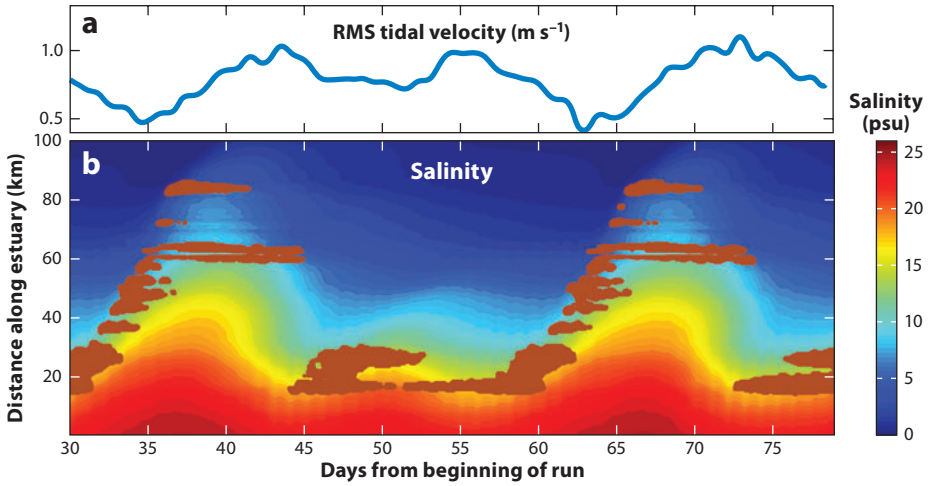

Figure 3

Model simulation of bottom salinity position in the Hudson River through several spring-neap cycles with constant river discharge and realistic topography. The brown shading indicates locations where $|\partial s/\partial x| > 0.5$ psu per kilometer. Note that the salinity gradient zone propagates landward during neap tides. Topographic variation favors frontogenesis at certain locations, most notably at approximately 20 and 60 km. Figure adapted from Ralston et al. (2012). Abbreviation: psu, practical salinity units; RMS, root mean square.

balance. The lateral structure of the estuarine circulation results mainly from lateral variations in the baroclinicity and stress distribution due to transverse depth variations (Wong 1994). Deeper sections tend to have stronger inflow owing to the greater net contribution of baroclinicity, with outflow occurring preferentially on the flanks (Fischer 1972, Wong 1994, Valle-Levinson et al. 2000). The net influence of the lateral variability on the estuarine circulation is an increase in the effective exchange flow for a given amount of baroclinic forcing because of the reduced influence of vertical mixing on the exchange flow when it is laterally segregated (Valle-Levinson 2008).

Within the tidal cycle, the lateral variation in depth produces the phenomenon of differential advection, in which stronger velocities in the deep channel result in a tidally modulated cross-estuary density gradient (Nunes & Simpson 1985). The cross-estuary density gradient induces a lateral circulation (Smith 1976, Nunes & Simpson 1985), which includes counter-rotating cells that carry surface water toward the center of the channel during the flood tide, with the reverse during the ebb tide. The surface convergence leads to distinctive axial convergence fronts, discussed by Nunes & Simpson (1985), which are often manifest as continuous filaments of foam and other flotsam snaking along the center of estuarine channels during flood tides. The lateral circulation also may lead to restratification of a well-mixed water column owing to lateral straining (Lacy et al. 2003, Scully & Geyer 2012).

Owing to both baroclinic effects and nonlinear advective processes, the lateral circulation tends to be much stronger during flood than ebb tides (Lerczak & Geyer 2004). This asymmetry in turn results in asymmetry in the along-estuary momentum balance. Lerczak & Geyer found that for a weakly stratified estuary, the tidal variation in lateral advection is a significant driving force for the estuarine circulation. Their numerical experiments were highly idealized, however, with the imposition of a constant eddy viscosity and a simple domain. Scully et al. (2009) confirmed the same result for a realistic simulation of the partially mixed Hudson River estuary, using stratification-dependent turbulence closure. In both the simplified and realistic domains, the strong secondary circulation during flood tides results in the advection of low-momentum fluid from the sides to the

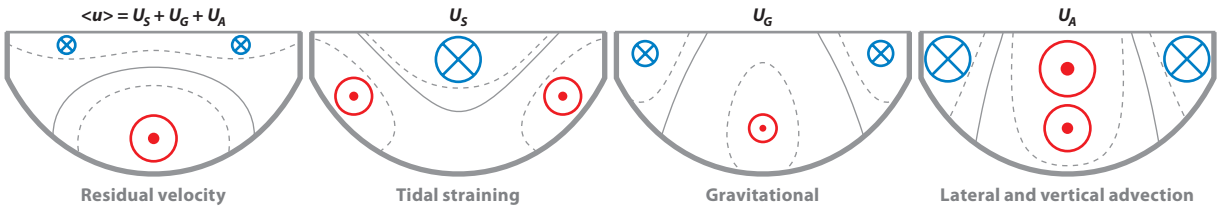

Figure 4

Sketch of the decomposed residual velocity components on a 2D cross section based on simulations of Burchard et al. (2011, figures 5 and 6). The parabolic channel shape tends to have the inflow in the deep central channel (the point of view is looking toward the ocean, so *red circles* are landward flow). The strain-induced circulation actually forces landward flow on the flanks. In terms of magnitude, the advectively induced circulation is the largest. Physically, the landward u_A in the deep central channel is forced by the convergence and downward advection of the flood momentum forced by lateral baroclinicity.

middle of the estuary, which slows down the near-surface current during the flooding tide. During the ebb tide, the weaker lateral circulation has minimal inhibiting influence on the shear. When averaged over the tidal cycle, the lateral advection is a source term for the estuarine circulation, converting the shear generated by barotropic flow into residual shear. The mechanism is analogous to the tidal straining circulation discussed in Section 3, but rather than turbulence causing the reduction of shear during the flood tide, the lateral circulation achieves the same result.

The 2D (y, z) modeling by Burchard et al. (2011) provides a detailed comparison of the influence of the lateral advective term relative to other contributors to the residual circulation. They used a parabolic channel, again with constant b_x. Their decomposition of the velocity is the same as in Equation 16, except that now the $\langle\eta\rangle$ gradients are adjusted to force zero section-averaged transport for each term. Also a new residual velocity u_A is introduced, forced by the lateral and vertical momentum advection according to

$$\partial u_A/\partial z = G_A z/\langle A\rangle + \left\{-\int_z^0 \langle vu\rangle_y d\hat{z} + \langle wu\rangle\right\}/\langle A\rangle. \qquad (17)$$

It has small influence for $Si < 0.1$, but it becomes one of the dominant terms when $Si \sim 0.2$ (**Figure 4**). At higher Si, when stratification is strong through the tidal cycle, Scully et al. (2009) found that the secondary circulation remains strong, but its influence on the residual diminishes because of the more complex vertical structure of the secondary flow. Burchard et al. found that its importance diminishes for greater unsteadiness owing to the tidal time dependence of the lateral baroclinicity. They also confirmed Lerczak & Geyer's result that the advective effect diminishes for a wider estuary, simply because advective gradients scale inversely with width.

Estuaries whose widths exceed the deformation scale $L_D \sim (g'H)^{1/2}/f$, where g' is the reduced gravity of the local stratification, exhibit another mode of lateral variability due to rotation (Valle-Levinson 2008). In essence, the outflow becomes a coastal current, traveling along the right-hand shore (in the Northern Hemisphere). Valle-Levinson's analysis indicates that the strength of the exchange flow has a complex dependence on width that also depends on the lateral shape and vertical mixing rate, so no general statement can be made about estuarine circulation being stronger in wide or narrow estuaries.

4.2. Along-Estuary Variability in the Circulation

The length of the salinity intrusion sets an along-estuary scale on the estuarine circulation (Chatwin 1976), in which there is a gradual, monotonic increase in the strength of the estuarine circulation

toward the mouth. In typical, partially mixed estuaries with weak to moderate tidal flow, that scale is tens of kilometers to 100 km, so the gradients in circulation at the estuary scale are modest. However, most estuaries are not longitudinally uniform channels and typically have curves, sills, and headlands at much smaller along-estuary scales than the overall estuary dimension. A large number of studies have addressed the impact of topographic variations on mixing (e.g., Partch & Smith 1978, Farmer & Smith 1980, Peters 1999, Klymak & Gregg 2004), but little attention has been given to the influence of along-estuary topographic variations on the estuarine circulation.

Several recent studies do shed light on the variability of the along-estuary circulation. The Strait of Juan de Fuca is a deep estuary with a pronounced exchange flow, the dynamics of which were not fully explained in previous investigations (Ott & Garrett 1998, Ott et al. 2002). Using a high-resolution 3D numerical model, Martin & MacCready (2011) found that the baroclinic pressure gradient actually changes sign along the estuary in response to topographic variability, at scales of 5 to 25 km. Their detailed analysis indicates that the sum of the pressure gradient, Coriolis acceleration, and advection is essentially constant, but the individual components (including the along-estuary advection term) fluctuate markedly in response to topographic variations. The estuarine transport also varies spatially but not as abruptly as the individual terms in the momentum balance. These results confirm the theoretical expectation that the tidally averaged Bernoulli function, $\langle \mathbf{u} \cdot \mathbf{u}/2 + p/\rho + gz \rangle$, where p is the pressure, can vary along the estuary mainly because of dissipative processes, which are relatively weak in this deep, stratified estuary. However, significant inviscid exchanges between kinetic and potential energy may occur over short spatial scales, linked to the geography of the strength of tidal currents. It is noteworthy that Pritchard (1956) anticipated the importance of $\langle u u_x \rangle$, but without access to high-resolution measurements or modeling, he could not substantiate the conjecture at that time.

Chen et al. (2012) found similar variability in the baroclinic pressure gradient in the much shallower Hudson River estuary. In this case, these baroclinic variations generated large along-estuary variations in the strength of the exchange flow (**Figure 5*b***). Jay & Smith (1990) also reported topographically induced variability of the residual in the Columbia estuary. The mechanism for these variations is similar to the Juan de Fuca situation—the flow over topography results in a large-amplitude response of the density interface owing to the near-critical Froude number (Farmer & Smith 1980), which in turn leads to significant variations in the vertical structure of the velocity in the vicinity of topography. These highly asymmetric tidal variations in the response to topography have a large impact on the Eulerian residual circulation, as demonstrated by Chen et al. Leading-order variations in the exchange flow would be expected to require large recirculations to conserve volume transport, but this is not the case—in fact, there is only modest recirculation associated with topography. It turns out that the correlation between interfacial displacements and tidal flow contributes a major fraction of the exchange flow (Geyer & Nepf 1996), so although the tidally averaged Eulerian exchange flow is highly variable, the exchange flow averaged over a specific density range is nearly constant through regions of abrupt topography, as explained in Section 4.3.

A study by Ralston et al. (2010) of the Merrimack River, a highly time-dependent salt-wedge estuary, also reveals strong along-estuary variation of the exchange flow. In this regime, unlike in the Hudson, most of the salt transport is associated with tidal variations in velocity and salinity rather than the mean Eulerian exchange flow owing to the along-estuary propagation of the salt front. The extreme variability of the salinity and velocity structure in estuaries whose length is comparable to the tidal excursion brings into question the approach of tidal averaging to determine residual quantities. In such estuaries with extreme tidal variability of salinity and velocity, the tidally averaged Eulerian quantities have little relevance to the overall momentum and salt balances. For regimes with moderate tidal variability such as the Hudson, or extreme cases like the Merrimack, the Eulerian exchange flow is of limited utility, and a more robust method is sought that provides

THE EULERIAN EXCHANGE FLOW

The term Eulerian exchange flow does not conform exactly to the accepted definition of an Eulerian reference frame (meaning fixed location) in fluid mechanics and is used here to contrast with the total exchange flow averaging method described in Section 4.3. The Eulerian exchange flow is the subtidal along-channel flow at some location on a cross section and is calculated as a transport velocity, meaning $\langle u\delta\rangle/\langle\delta\rangle$, where δ is an element of the sectional area. δ is allowed to vary in time as the tide height on the section changes, such that there is a constant number of area elements between the instantaneous top and bottom, like sigma coordinates in numerical models. This transport velocity thus incorporates the Stokes drift due to tidal variation of the surface height, an important consideration for data processing in systems with large tidal range (Lerczak et al. 2006).

a quantification of the exchange flow in the presence of significant spatial and temporal variability. The total exchange flow (TEF) method described below may provide this.

4.3. Calculating the Total Exchange Flow Using Isohaline Coordinates

The global salt balance (Equation 10) is a primary motivation for the study of the physics of the residual circulation $\langle u\rangle$ detailed above. The salt flux relies in part on the spatial correlation of $\langle u\rangle$ and $\langle s\rangle$, but the final term in Equation 10 accounts for temporal (especially tidal) correlations, and it is often important as well. As an alternative to the Eulerian methods, several recent studies (MacCready 2011, Sutherland et al. 2011, Chen et al. 2012) have expanded on the method of MacDonald & Horner-Devine (2008) in which subtidal transport is calculated as a function of salinity instead of spatial position. Let us define the subtidal transport

$$Q(s) \equiv \left\langle \int_{A_S} ud\,A \right\rangle \tag{18}$$

of all the water with salinity greater than s (**Figure 5*a***). Then the volume flux as a function of salinity is $-\partial Q/\partial s$, and the inflowing volume transport of the exchange flow is given by

$$Q_{\rm in} \equiv \int -\partial Q/\partial s|_{\rm in}\, ds\,. \tag{19}$$

The analogous outflow, $Q_{\rm out}$, has magnitude $Q_{\rm in} + Q_R$ to conserve volume, where Q_R is the river volume flux. We may also define the flux-weighted salinity of both streams of the exchange flow, $S_{\rm in}$ and $S_{\rm out}$, and $\Delta S \equiv S_{\rm in} - S_{\rm out}$ is a measure of the stratification. Together, these terms are called the TEF in MacCready (2011). Chen et al. (2012) found that $Q_{\rm in}$ varies smoothly in x, with a near-monotonic increase toward the mouth. In contrast, an Eulerian version of this transport, calculated using subtidal velocity and salinity, shows much greater spatial variability (**Figure 5*b***). This Eulerian variability constitutes not variations in the actual volume transport or salt flux but rather variations in the partitioning between the Eulerian mean and the tidal pumping component (the tidal correlation term in Equation 10). The TEF analysis suggests that the tidal pumping component, which is often parameterized as a Fickian diffusion term (Hansen & Rattray 1965, MacCready 1999), is actually part of the exchange flow that has been distorted in the Eulerian reference frame by tidal variability of the salinity structure. Although this line of analysis is only just beginning, the results suggest that TEF provides a more robust and kinematically accurate means of quantifying the exchange flow than Eulerian time averaging.

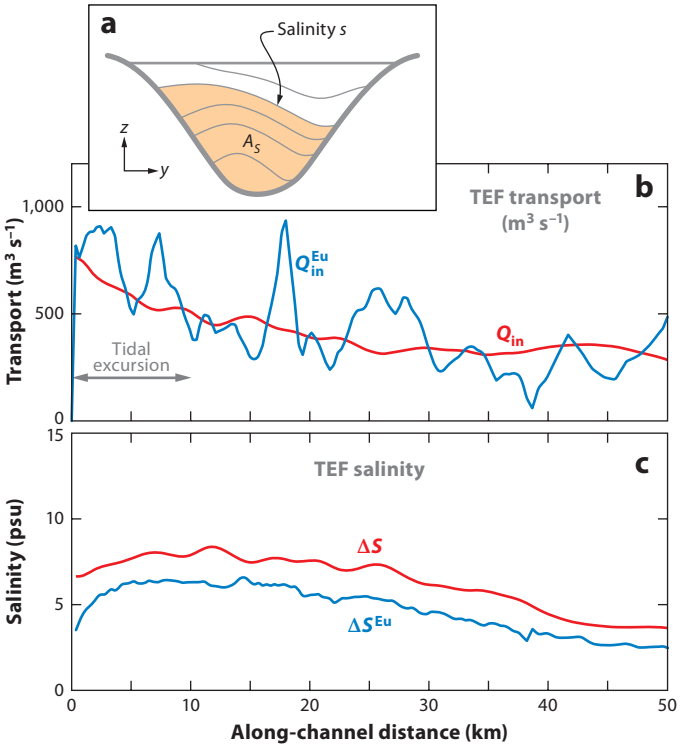

Figure 5

Total exchange flow (TEF) from an analysis of a numerical model of the partially mixed Hudson estuary. (*a*) Definition sketch for the isohaline TEF analysis. (*b*) The isohaline inflow, Q_{in}, based on TEF analysis plotted versus distance (*red line*) and the Eulerian inflow, Q_{in}^{Eu}, calculated from tidally averaged fields (*blue line*). The extreme variability in the Eulerian transport relative to Q_{in} results from the varying contributions of tidal and Eulerian residual transport due to the interaction of the flow with topography. (*c*) The TEF stratification, $\Delta S = S_{in} - S_{out}$, showing a gradual increase toward the mouth. The analogous Eulerian version is smaller everywhere, meaning that the residual underrepresents the full range of salinity participating in the exchange flow. Panels *b* and *c* adapted with permission from Chen et al. (2012), copyright American Meteorological Society. Abbreviation: psu, practical salinity units.

5. THE ESTUARINE PARAMETER SPACE

A perennial challenge in advancing estuarine dynamics is the vast range of conditions among estuaries, which impedes the generalization of results. Numerous authors have developed parameterizations of estuarine variables in attempts to classify estuaries, with the two-parameter classification scheme of Hansen & Rattray (1966) the most frequently cited. These authors used the stratification and circulation as the two dimensions of the classification scheme and then used analytic expressions derived from Hansen & Rattray's (1965) similarity solution to map the forcing variables, such as tidal currents and river flow, onto the diagram. In spite of its longevity, Hansen & Rattray's scheme is seriously compromised by the inherent variability of estuarine stratification and circulation, either one of which could vary by an order of magnitude within the spring-neap cycle.

An alternative approach is to map the estuarine parameter space based on the principal forcing variables, the tidal velocity and the freshwater flow, with appropriate nondimensionalization. Geyer (2010) proposed such a scheme with the freshwater Froude number,

$Fr_f = U_R/(\beta g s_{\text{ocean}} H)^{1/2}$, the net velocity due to river flow scaled by the maximum possible frontal propagation speed, with a tidal Froude number as the other axis. Although this approach is reasonably effective at separating different estuarine regimes, it is limited in its ability to address the key issues of mixing and the dynamics of the tidal straining circulation. Recent studies by Burchard and colleagues demonstrate the importance of time dependence for estuarine dynamics, as represented by their unsteadiness number, *Un* (Equation 14), introduced in Section 3. However, *Un* does not account for the influence of stratification expressed in the equation for vertical mixing (Equation 13). Based on Equation 13, a mixing parameter can be defined that quantifies the effectiveness of tidal mixing for a stratified estuary:

$$M^2 = \frac{C_D U_T^2}{\omega N_o H^2}, \tag{20}$$

where $N_o = (\beta g s_{\text{ocean}}/H)^{1/2}$ is the buoyancy frequency for maximum top-to-bottom salinity variation in an estuary. The critical mixing condition from Equation 13 then becomes

$$\left(\frac{s_{\text{ocean}}}{\delta s_i}\right)^{1/2} M^2 \approx 1, \tag{21}$$

where δs_i is the initial vertical salinity difference (e.g., at the beginning of the flood or ebb tide). *M* provides an alternative means of nondimensionalizing the tidal velocity with direct relevance to the effectiveness of vertical mixing, as M^2 can be regarded as the ratio of the tidal timescale to the vertical mixing timescale.

A mapping of various estuaries onto the two-parameter Fr_f-*M* space (**Figure 6**) indicates that these variables provide an effective means of discriminating different classes of estuaries. Partially mixed estuaries such as the Hudson and the James River fall in the middle of the diagram. Salt-wedge estuaries such as the Mississippi and the Ebro River are near the top, and time-dependent salt wedges such as the Fraser and Merrimack River are in the upper-right corner. Fjords, by virtue of their great depth, which reduces both tidal and freshwater velocity scales, fall in the lower-left corner of the diagram. Well-mixed and nearly well-mixed SIPS (Simpson et al. 1990) estuaries fall in the lower-right quadrant.

Analytic solutions for idealized estuaries (cf. Section 2) can be used to discern the structure of this parameter space, even though these solutions should be considered qualitative. As discussed in Section 2, steady-state estuarine scaling for gravitationally driven circulation leads to a stratification that scales as $Fr_f^{2/3}$ (MacCready 1999), consistent with the general tendency for stratification to increase moving upward on the diagram. Using MacCready's (1999) equation for stratification that $\delta s/s_{\text{ocean}} = \alpha\, Fr_f^{2/3}$, where $\alpha = 3.4$ based on Geyer's (2010) empirical fit to a number of estuaries, and substituting into Equation 21, we obtain the condition for vertical mixing:

$$\alpha^{1/2} Fr_f^{1/3} M^2 \approx 1. \tag{22}$$

The diagonal mixing line through the middle of the parameter space divides the estuaries (of a given *H*) that should always remain stratified from those in which boundary-generated mixing reaches the surface within a tidal cycle. Estuaries below this line may not mix completely, but the boundary-generated stress will extend through the water column. The position in parameter space at which complete mixing should occur within a tidal cycle is not determined from analytical calculations but is based empirically on conditions in San Francisco Bay (Stacey et al. 2001) and the numerical models of Cheng et al. (2010) and Burchard et al. (2011).

We note that estuaries are not points but are rather rectangles in parameter space, owing to the spring-neap variations in the tidal velocity (resulting in a range in *M*) and seasonal or event-driven changes in river flow (producing a range in Fr_f). Significant variations in depth (e.g.,

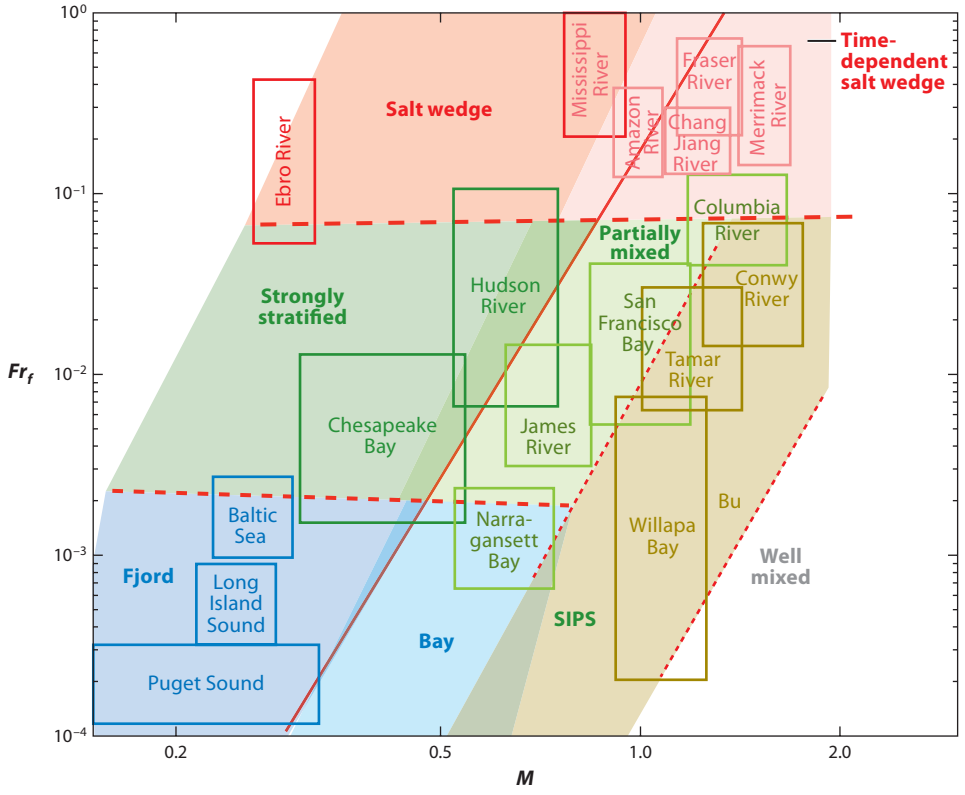

Figure 6

Estuarine parameter space, based on the freshwater Froude number and mixing number. The solid red diagonal line indicates the value of M at which the tidal boundary layer can reach the surface (based on Equation 13, using an analytical relation between Fr_f and stratification). Each rectangle indicates the approximate influence of spring-neap tidal variation, river flow variation, and bathymetric variation for the estuaries indicated. Bu represents the location of Burchard et al.'s (2011) simulations. Abbreviation: SIPS, strain-induced periodic stratification.

Puget Sound and Chesapeake Bay) also result in a range in M. Many partially mixed estuaries (notably, the Hudson River, James River, Chesapeake Bay, and San Francisco Bay) cross over during the spring-neap cycle between different estuarine types. Some partially mixed estuaries also cross into the salt-wedge classification during high flow conditions. Burchard et al.'s (2011) simulations are found at the weakly stratified edge of the SIPS regime, similar to Willapa Bay at spring tides.

Based on the importance of Si for the dynamics of both gravitational and tidal straining circulations, the reader may ask why Si was not selected as one of the nondimensional variables. The answer is twofold. First, Si includes the along-estuary density gradient, which is a key dependent variable in the coupled equations for the estuarine circulation. Second, the values of Si vary greatly within one estuary as a function of time and space, mainly because of the variability of $\partial s/\partial x$, as discussed in the last section. The general tendency is for Si to be lowest for the well-mixed systems (i.e., the lower-right corner of the Fr_f-M space in **Figure 6**), ranging from 0.1 to 0.3 in the SIPS band, 0.3 to 0.5 in the partially mixed zone, and for it to be generally higher but more variable in

the more stratified parts of parameter space. Time-dependent salt wedges as well as fjords show large variability in *Si*, probably because of the frontal nature of these regimes.

One conclusion of this mapping of estuarine parameter space is that estuaries exhibit great diversity in regimes, depending on the strength of the two key forcing agents—the river flow and tidal currents. Many estuaries reside near the transition between stable, stratified conditions and well-mixed conditions, and the spring-neap variation of tides (represented by the span of M for each estuary) is in many cases large enough for estuaries to cross boundaries between regimes. The particular sensitivity of estuarine stratification to the spring-neap variation in mixing intensity explains the failure of previous classification schemes based on stratification. In fact, the recent literature argues that the variability of the circulation and stratification of estuaries at tidal and spring-neap timescales is fundamentally important to the time-average momentum and salt balances.

6. CONCLUSIONS AND UNRESOLVED QUESTIONS

This review documents recent research on the estuarine circulation that challenges the classic model of a steady, baroclinically driven exchange flow. These studies emphasize the importance of the mixing timescale relative to the tidal timescale, which can be parameterized by the mixing parameter M. As M increases above 1, the mixing timescale becomes shorter than the tidal timescale, and alternation between stratified and mixed conditions is correlated with the tidal flow, resulting in the tidal straining circulation, which is driven in large part by the rectification of the tide-induced shear. The estuaries that exhibit this mode of circulation have relatively weak freshwater forcing, represented in the lower-right quadrant of the Fr_f-M parameter space in **Figure 6**. As the timescale of tidal mixing increases, estuaries exhibit the more familiar partially mixed regime, in which the baroclinic pressure gradient is the main driver of the residual, although tidal advection is also a key player in the residual momentum balance. The time dependence of mixing is still important in this regime as well, although it is expressed at spring-neap timescales, often resulting in runaway stratification and enhanced exchange flow during neap tides and weakened stratification and circulation during spring tides.

Another class of estuaries that has recently received attention is the time-dependent salt wedge, which resides in the upper-right corner of the Fr_f-M space in **Figure 6**, being strongly forced by tides and river flow. Rather than occurring as a result of rapid vertical mixing, tidal variation occurs because the length of the salt intrusion is comparable to the length of the tidal excursion, so the tidal advection of the salt wedge results in extreme tidal variability of the velocity and salinity structure. These short, highly variable systems present a significant challenge to the estimation of an Eulerian exchange flow. Likewise, estuaries subject to significant topographic forcing exhibit complex and variable Eulerian exchange flow, owing to the varying contribution of tidal and mean Eulerian salt fluxes. The quasi-Lagrangian TEF provides an effective means of quantifying the estuarine circulation in spatially complex regimes with strong tidal forcing.

The broad recognition of the importance of time dependence from tidal to spring-neap timescales leads to a revised view of the mechanisms by which estuaries maintain their salt balance. Estuaries appear to be in a continual state of adjustment to changes in the tidal forcing conditions, either within the tidal cycle or within the spring-neap cycle. Instead of viewing estuaries as exhibiting a steady, advective-diffusive salt balance, they are more realistically represented as alternating between gravity-current pulses and mixing events. The timescale of pulsing may be as little as 1–2 h during the change of the tide, as exhibited in San Francisco Bay (Stacey et al. 2001), or may be the entire duration of the neap tide, as data and models of the Hudson River estuary suggest (Ralston et al. 2008, 2012) (**Figure 3**). The pulsing is reminiscent of experiments

by Simpson & Linden (1989) in which they generated gravity currents by reducing mixing in regions of intensified horizontal density gradients. This process of frontogenesis is likely an essential ingredient of the transition from mixed to stratified conditions in estuaries as well as a major contributor to the exchange flow.

Future research in estuarine circulation will benefit tremendously by the joint application of advanced measurements and 3D numerical models. Some recent advances in our understanding of the momentum balance and time-dependent salt fluxes have benefitted from this combination, but fundamental questions remain that are readily addressed with the present generation of models and measurement techniques. Investigations of the along-estuary structure have lagged behind relative to the attention to vertical and lateral structure. The problem of frontogenesis mentioned in the last paragraph is ripe for combined field and numerical investigations. The hydraulics of estuarine flows, highlighted in studies of fjord dynamics (Stigebrandt 1981, Gregg & Pratt 2010), have not received adequate attention in estuarine research, yet this approach offers considerable potential for addressing the interactions between estuarine flows and topography in all stratified estuaries. The study of mixing processes has been and will continue to be a critical avenue of estuarine research, particularly in context with the increased spatial resolution of models that approach the scales of the mixing processes themselves.

The diversity of estuarine environments can be a hindrance to research, particularly if the estuary's location in parameter space is inadequately specified. However, as the parameter space becomes better defined, the commonality of processes among estuaries will be better appreciated, and progress in our understanding of estuarine processes will accelerate. The surprisingly late identification of the importance of the tidal frequency in estuarine dynamics helps to spread out the parameter space to reveal new distinctions among estuarine regimes. A more accurate map of parameter space not only helps inform comparisons between estuaries, it also provides predictions of transitions within individual estuaries as forcing conditions change. As field and modeling programs generate ever greater volumes of data, the need for collapsing those data within a dynamically relevant framework becomes all the more important.

DISCLOSURE STATEMENT

The authors are not aware of any biases that might be perceived as affecting the objectivity of this review.

ACKNOWLEDGMENTS

W.R.G. was supported by NSF grant OCE-1232928, and P.M. was supported by NSF grant OCE-0849622.

LITERATURE CITED

Burchard H, Hetland RD. 2010. Quantifying the contributions of tidal straining and gravitational circulation to residual circulation in periodically stratified tidal estuaries. *J. Phys. Oceanogr.* 40:1243–62

Burchard H, Hetland RD, Schulz E, Schuttelaars HM. 2011. Drivers of residual estuarine circulation in tidally energetic estuaries: straight and irrotational channels with parabolic cross section. *J. Phys. Oceanogr.* 41:548–70

Chatwin PC. 1976. Some remarks on the maintenance of the salinity distribution in estuaries. *Estuar. Coast. Mar. Sci.* 4:555–66

Chen SN, Geyer WR, Ralston DK, Lerczak JA. 2012. Estuarine exchange flow quantified with isohaline coordinates: contrasting long and short estuaries. *J. Phys. Oceanogr.* 42:748–63

Cheng P, Valle-Levinson A, de Swart HE. 2010. Residual currents induced by asymmetric tidal mixing in weakly stratified narrow estuaries. *J. Phys. Oceanogr.* 40:2135–47
Dyer KR, Soulsby RL. 1988. Sand transport on the continental shelf. *Annu. Rev. Fluid Mech.* 20:295–324
Farmer DM, Smith JD. 1980. Tidal interaction of stratified flow with a sill in Knight Inlet. *Deep Sea Res. A* 27:239–54
Feely RA, Alin SR, Newton J, Sabine CL, Warner M, et al. 2010. The combined effects of ocean acidification, mixing, and respiration on pH and carbonate saturation in an urbanized estuary. *Estuar. Coast. Shelf Sci.* 88:442–49
Fischer HB. 1972. Mass transport mechanisms in partially stratified estuaries. *J. Fluid Mech.* 53:671–87
Geyer WR. 2010. Estuarine salinity structure and circulation. In *Contemporary Issues in Estuarine Physics*, ed. A Valle-Levinson, pp. 12–26. Cambridge, UK: Cambridge Univ. Press
Geyer WR, Cannon GA. 1982. Sill processes related to deep water renewal in a fjord. *J. Geophys. Res.* 87:7985–96
Geyer WR, Nepf HM. 1996. Tidal pumping of salt in a moderately stratified estuary. *Coast. Estuar. Stud.* 53:213–26
Geyer WR, Trowbridge JH, Bowen MM. 2000. The dynamics of a partially mixed estuary. *J. Phys. Oceanogr.* 30:2035–48
Gregg MC, Pratt LJ. 2010. Flow and hydraulics near the sill of Hood Canal, a strongly sheared, continuously stratified fjord. *J. Phys. Oceanogr.* 40:1087–105
Griffin DA, LeBlond PH. 1990. Estuary/ocean exchange controlled by spring-neap tidal mixing. *Estuar. Coast. Shelf Sci.* 30:275–97
Haas LW. 1977. The effect of the spring-neap tidal cycle on the vertical salinity structure of the James, York and Rappahannock rivers, Virginia, USA. *Estuar. Coast. Mar. Sci.* 4:485–96
Hansen DV, Rattray M. 1965. Gravitational circulation in straits and estuaries. *J. Mar. Res.* 23:104–22
Hansen DV, Rattray M. 1966. New dimensions in estuary classification. *Limnol. Oceanogr.* 11:319–26
Hetland RD, Geyer WR. 2004. An idealized study of the structure of long, partially mixed estuaries. *J. Phys. Oceanogr.* 34:2677–91
Hopkinson CS, Giblin AE, Tucker J, Garritt RH. 1999. Benthic metabolism and nutrient cycling along an estuarine salinity gradient. *Estuar. Coasts* 22:863–81
Hughes FW, Rattray M. 1980. Salt flux and mixing in the Columbia River estuary. *Estuar. Coast. Mar. Sci.* 10:479–93
Jay DA, Musiak JD. 1994. Particle trapping in estuarine tidal flows. *J. Geophys. Res.* 99:20445–61
Jay DA, Smith JD. 1990. Circulation, density distribution and neap-spring transitions in the Columbia River estuary. *Prog. Oceanogr.* 25:81–112
Kato H, Phillips OM. 1969. On the penetration of a turbulent layer into stratified fluid. *J. Fluid Mech.* 37:643–55
Klymak JM, Gregg MC. 2004. Tidally generated turbulence over the Knight Inlet sill. *J. Phys. Oceanogr.* 34:1135–51
Lacy JR, Stacey MT, Burau JR, Monismith SG. 2003. Interaction of lateral baroclinic forcing and turbulence in an estuary. *J. Geophys. Res.* 108:3089
Lerczak JA, Geyer WR. 2004. Modeling the lateral circulation in straight, stratified estuaries. *J. Phys. Oceanogr.* 34:1410–28
Lerczak JA, Geyer WR, Chant RJ. 2006. Mechanisms driving the time-dependent salt flux in a partially stratified estuary. *J. Phys. Oceanogr.* 36:2296–311
Lerczak JA, Geyer WR, Ralston DK. 2009. The temporal response of the length of a partially stratified estuary to changes in river flow and tidal amplitude. *J. Phys. Oceanogr.* 39:915–33
Li M, Zhong L. 2009. Flood-ebb and spring-neap variations of mixing, stratification and circulation in Chesapeake Bay. *Cont. Shelf Res.* 29:4–14
MacCready P. 1999. Estuarine adjustment to changes in river flow and tidal mixing. *J. Phys. Oceanogr.* 29:708–26
MacCready P. 2004. Toward a unified theory of tidally-averaged estuarine salinity structure. *Estuaries* 27:561–70

MacCready P. 2007. Estuarine adjustment. *J. Phys. Oceanogr.* 27:2133–45
MacCready P. 2011. Calculating estuarine exchange flow using isohaline coordinates. *J. Phys. Oceanogr.* 41:1116–24
MacCready P, Geyer WR. 2010. Advances in estuarine physics. *Annu. Rev. Mar. Sci.* 2:35–58
MacDonald DG, Horner-Devine AR. 2008. Temporal and spatial variability of vertical salt flux in a highly stratified estuary. *J. Geophys. Res.* 113:C09022
Malone TC, Crocker LH, Pike SE, Wendler BW. 1988. Influences of river flow on the dynamics of phytoplankton production in a partially stratified estuary. *Mar. Ecol. Prog. Ser.* 48:235–49
Martin WD, MacCready P. 2011. Influence of large-scale tidal asymmetry on subtidal dynamics in the western Strait of Juan de Fuca. *J. Geophys. Res.* 116:C02009
Monismith SG, Burau JR, Stacey MT. 1996. Stratification dynamics and gravitational circulation in northern San Francisco Bay. In *San Francisco Bay: The Ecosystem*, ed. T Hollibaugh, pp. 1–31. Ashland, OR: Pac. Div. Am. Assoc. Adv. Sci.
Monismith SG, Kimmerer W, Burau JR, Stacey MT. 2002. Structure and flow-induced variability of the subtidal salinity field in northern San Francisco Bay. *J. Phys. Oceanogr.* 32:3003–18
Nezu I, Rodi W. 1986. Open-channel flow measurements with a laser Doppler anemometer. *J. Hydraul. Eng.* 112:335–55
Nunes RA, Simpson JH. 1985. Axial convergence in a well-mixed estuary. *Estuar. Coast. Shelf Sci.* 20:637–49
Nunes Vaz RA, Lennon GW, de Silva Samarasinghe JR. 1989. The negative role of turbulence in estuarine mass transport. *Estuar. Coast. Shelf Sci.* 28:361–77
Ott MW, Garrett C. 1998. Frictional estuarine flow in Juan de Fuca Strait, with implications for secondary circulation. *J. Geophys. Res.* 103:15657–66
Ott MW, Dewey R, Garrett C. 2002. Reynolds stresses and secondary circulation in a stratified rotating shear flow. *J. Phys. Oceanogr.* 32:3249–68
Paerl HW, Pinckney JL, Fear JM, Peierls BL. 1998. Ecosystem responses to internal and watershed organic matter loading: consequences for hypoxia in the eutrophying Neuse River Estuary, North Carolina, USA. *Mar. Ecol. Prog. Ser.* 166:17–25
Partch EN, Smith JD. 1978. Time dependent mixing in a salt wedge estuary. *Estuar. Coast. Mar. Sci.* 6:3–19
Peters H. 1999. Spatial and temporal variability of turbulent mixing in an estuary. *J. Mar. Res.* 57:805–45
Peters H, Bokhorst R. 2001. Microstructure observations of turbulent mixing in a partially mixed estuary. Part II: salt flux and stress. *J. Phys. Oceanogr.* 31:1105–19
Pritchard DW. 1956. The dynamic structure of a coastal plain estuary. *J. Mar. Res.* 15:33–42
Ralston DK, Geyer WR, Warner JC. 2012. Bathymetric controls on sediment transport in the Hudson River estuary: lateral asymmetry and frontal trapping. *J. Geophys. Res.* 117:C10013
Ralston DK, Geyer WR, Lerczak JA. 2008. Subtidal salinity and velocity in the Hudson River estuary: observations and modeling. *J. Phys. Oceanogr.* 28:753–70
Ralston DK, Geyer WR, Lerczak JA. 2010. Structure, variability, and salt flux in a strongly forced salt wedge estuary. *J. Geophys. Res.* 115:C06005
Scully ME, Geyer WR. 2012. The role of advection, straining, and mixing on the tidal variability of estuarine stratification. *J. Phys. Oceanogr.* 42:855–68
Scully ME, Geyer WR, Lerczak JA. 2009. The influence of lateral advection on the residual estuarine circulation: a numerical modeling study of the Hudson River estuary. *J. Phys. Oceanogr.* 39:107–24
Scully ME, Geyer WR, Trowbridge JH. 2011. The influence of stratification and nonlocal turbulent production on estuarine turbulence: an assessment of turbulence closure with field observations. *J. Phys. Oceanogr.* 41:166–85
Sharples J, Simpson JH. 1993. Periodic frontogenesis in a region of freshwater influence. *Estuar. Coasts* 16:74–82
Simpson JH, Brown J, Matthews J, Allen G. 1990. Tidal straining, density currents, and stirring in the control of estuarine stratification. *Estuaries* 13:125–32
Simpson JE, Linden PF. 1989. Frontogenesis in a fluid with horizontal density gradients. *J. Fluid Mech.* 202:1–16
Smith R. 1976. Longitudinal dispersion of a buoyant contaminant in a shallow channel. *J. Fluid Mech.* 78:677–88

Stacey MT. 1996. *Turbulent mixing and residual circulation in a partially stratified estuary*. PhD diss. Stanford Univ., Stanford, CA. 209 pp.
Stacey MT, Brennan ML, Burau JR, Monismith SG. 2010. The tidally averaged momentum balance in a partially and periodically stratified estuary. *J. Phys. Oceanogr.* 40:2418–34
Stacey MT, Burau J, Monismith SG. 2001. Creation of residual flows in a partially stratified estuary. *J. Geophys. Res.* 106:17013–37
Stacey MT, Ralston DK. 2005. The scaling and structure of the estuarine bottom boundary layer. *J. Phys. Oceanogr.* 35:55–71
Stigebrandt A. 1981. A mechanism governing the estuarine circulation in deep, strongly stratified fjords. *Estuar. Coast. Mar. Sci.* 13:197–211
Sutherland DA, MacCready P, Banas NS, Smedstad LF. 2011. A model study of the Salish Sea estuarine circulation. *J. Phys. Oceanogr.* 41:1125–43
Traykovski P, Geyer WR, Sommerfield C. 2004. Rapid sediment deposition and fine-scale strata formation in the Hudson estuary. *J. Geophys Res.* 109:F02004
Trowbridge JH. 1992. A simple description of the deepening and structure of a stably stratified flow driven by a surface stress. *J. Geophys. Res.* 97:15529–43
Umlauf L, Burchard H. 2005. Second-order turbulence closure models for geophysical boundary layers: a review of recent work. *Cont. Shelf Res.* 25:795–827
Uncles RJ, Stephens JA. 1993. The freshwater-saltwater interface and its relationship to the turbidity maximum in the Tamar estuary, United Kingdom. *Estuar. Coasts* 16:126–41
Valle-Levinson A. 2008. Density-driven exchange flow in terms of the Kelvin and Ekman numbers. *J. Geophys. Res.* 113:C04001
Valle-Levinson A. 2010. Definition and classification of estuaries. In *Contemporary Issues in Estuarine Physics*, ed. A Valle-Levinson, pp. 1–11. Cambridge, UK: Cambridge Univ. Press
Valle-Levinson A, Wong K-C, Lwiza KMM. 2000. Fortnightly variability in the transverse dynamics of a coastal plain estuary. *J. Geophys. Res.* 105:3413–24
van Aken HM. 1986. The onset of seasonal stratification in shelf seas due to differential advection in the presence of a salinity gradient. *Cont. Shelf Res.* 5:475–85
Warner JC, Geyer WR, Lerczak JA. 2005. Numerical modeling of an estuary: a comprehensive skill assessment. *J. Geophys. Res.* 110:C05001
Wong K-C. 1994. On the nature of transverse variability in a coastal plain estuary. *J. Geophys. Res.* 99:14209–22

Annual Review of
Fluid Mechanics

Volume 46, 2014

Contents

Indexes

Errata

An online log of corrections to *Annual Review of Fluid Mechanics* articles may be found at http://fluid.annualreviews.org/errata.shtml